Hary *et al.*
Acta Neuropathologica Communications (2025) 13:44
https://doi.org/10.1186/s40478-025-01957-6

Acta Neuropathologica Communications

RESEARCH

Open Access

Locus coeruleus tau validates and informs high-resolution MRI in aging and at earliest Alzheimer's pathology stages

Alexander T. Hary[1], Smriti Chadha[1], Nathaniel Mercaldo[1,3], Erin-Marie C. Smith[1], André J. W. van der Kouwe[1,2], Bruce Fischl[1,3], Christopher Mount[4], Liana Kozanno[4], Matthew P. Frosch[2,4] and Jean C. Augustinack[1,2*]

Abstract

The locus coeruleus (LC) has been identified as a site that develops phosphorylated tau pathology earlier than cerebral cortex. We present data using high-resolution postmortem MRI and validated tau histopathology in controls and the *earliest* Braak and Braak (BB) stages (BBI-BBII) in LC. The high-resolution ex vivo MRI provides a 3D volume (quantitative), while the histology reveals tau specificity and severity burden (semi-quantitative). We mapped our highly regionally specific LC data onto high-resolution 3D MRI reconstructions of the same samples used in histology (n = 11). We noted significant structural subatrophy between BB 0 and II (30.0% smaller volumes, $p = 0.0381$), a trend which primarily affected the rostral-most LC (49.2% smaller average volume, $p = 0.0381$). We show histopathology data on both the LC and neighboring dorsal raphe caudal (DRc), which were assessed at multiple rostrocaudal levels and mapped with highly sensitive tau severity spatial matrices. We observed significant LC tau accumulation between BB I and II (37.6% increase, $p < 0.0001$), which may reflect pathology change prior to presumptive cognitive impairment at BB III. Tau pathology was most severe in the middle portion of the LC (11.3% greater compared to rostral LC, $p = 0.0289$) when including BB III. We noted a significant rostrocaudal gradient of DRc tau severity (58.2% decrease between rostral and caudal DRc, $p < 0.0001$), suggesting selective regional vulnerabilities of both nuclei. Our study represents a rigorous approach to investigating LC and DRc pathology, having multiple histology sections per sublevel and high-resolution MRI to measure the whole LC, without missing slices in a histological only approach. Taken together, our findings provide novel validated data that demonstrate the tau pathology occurring in the LC and DRc during preclinical AD stages, and alongside spatial reconstructions that will serve as valuable references for in vivo LC imaging.

Keywords Brainstem, Upper pons, Locus coeruleus, Dorsal raphe nucleus, Early tau pathology, Spatial temporal heatmap, Subfields, Preclinical

*Correspondence:
Jean C. Augustinack
jaugustinack@mgh.harvard.edu
Full list of author information is available at the end of the article

Introduction

Brainstem nuclei—the norepinephrinergic locus coeruleus (LC) and the serotonergic dorsal raphe (DR) nuclei—with broad cortical projections [4, 53, 54] have been identified as sites that exhibit abnormally phosphorylated tau prior to its manifestation in cortex in Alzheimer's disease [17, 29, 33, 34, 66, 67]. Due to this early pathology, the LC and DR have become target areas for understanding AD in its preclinical stages.

The LC is the sole source of norepinephrinergic innervation to the cerebral cortex, including the hippocampus, and regulates attention [75], learning [8], memory formation and retrieval [64], and healthy sleep–wake cycles [71]. These functions, normally modulated by the LC, show impairment in the early stages of AD progression [25, 48, 50, 64]. The LC may be directly involved in slowing pathological progression, as norepinephrine plays a neuroprotective role for its efferents [37, 57]. In turn, a measure of LC health is its level of neuromelanin pigmentation, a byproduct of norepinephrine production. Neuromelanin is visible in histology, involved in reducing oxidative stress through heavy metal binding [58, 79], and creates natural contrast in MRI [15, 39, 41]. Hypopigmentation, a sign of LC integrity that can be assessed in vivo, is more common in AD [72], sleep dysfunction [72], and is linked to cortical microstructure damage [70]. LC bioimaging serves as a non-invasive method to assess LC integrity and is linked to several AD pathological and symptomatic changes [14, 19, 20, 24, 30, 38, 40, 45]. These studies have begun to identify LC characteristics and changes that may be indicative of early AD.

Moreover, AD pathology in the LC adopts a topographical pattern pertinent to its connectivity. Previous studies have reported more severe tau pathology in the cortically projecting [74] rostral- [73] and middle-most [28] portions of the LC as well as greater neuronal loss in the same regions [21, 69]. This makes regionality a highly relevant and trackable feature in LC pathology. Studies investigating DR pathology in AD report no similar rostrocaudal pathological gradient to that observed in the LC [28, 62]. Tau pathology is an early event in the LC and DR, warranting investigation in aging and the early stages of AD pathology, especially in LC.

Here, we seek to investigate the LC using ultra-high-resolution ex vivo MRI for volume measures, validated with tau histopathology in the same cases and at early Braak and Braak (BB) stages. This study focuses on the early timeline of Alzheimer's disease progression prior to symptom onset. We provide ground truth for the early histopathology, document the preclinical window with respect to these brainstem nuclei, and implement a systematic, rigorous approach to assess the tau pathology sub-topography in both the LC and the caudal DR subnucleus (DRc) with 3D isotropic MRI reconstructions.

Methods

Samples

We studied 21 human brain hemispheres, which were received from the Autopsy Suite at the Department of Neuropathology at Massachusetts General Hospital (Boston, MA). All samples were collected with consent in accordance with the Institutional Review Board of the Massachusetts General Hospital. Experiments met ethical standards guided by the Institutional Review Board. Samples were from individuals without cognitive impairment at the time of death. Causes of death were non-neurological and included cancer, cardiac death, and surgical complications. Healthy brain weights range between 1100 and 1600 g [11, 63]; our samples' brain weights were within this range (Table 1). The samples comprised 15 males and six females with mean age ± s.d., 65.4 ± 8.27. The distribution of the left and right hemispheres was eight and 13, respectively. Samples were fixed in 10% formalin and stored in 2% periodate-lysine-paraformaldehyde solution at 4° Celsius prior to any processing. While most cases included both MRI and histology data, five samples (#6, 10, 14, 17 and 19) had MRI only, and five samples (#1, 7, 8, 12 and 16) had histology only. Nine samples had DRc data. Sample demographic information is recorded in Table 1.

Ex vivo MRI acquisition

Ex vivo samples were imaged at 7 T with a Siemens Magnetom (Siemens Healthineers, Erlangen, Germany). Two types of radio frequency coils were used: a 31-channel phased array coil [27] and a 4-turn solenoid coil [6]. MRI resolution was ultra-high-resolution, typically at 120 μm, but ranged from 100 to 200 μm. All samples were at isotropic spatial resolutions. Table 1 displays the MRI resolution for each sample. Most samples (n = 14) were scanned as intact single hemispheres, while two samples were blocked and scanned as brainstems only with the cerebellum removed. Tissue blocks were packed and scanned in either 2% periodate-lysine-paraformaldehyde (n = 14) or Fomblin (n = 2, samples #2 and 4, YL VAC 06/6, Syensqo, Brussels, Belgium). A fast-low-angle-shot (FLASH) sequence with 3D encoding and a flip angle of 20° (range 10–30°) was implemented. The echo times (TE) were between 5.57 and 30 ms, and repetition times (TR) were between 32 and 60 ms, with bandwidths ranging from 20 to 180 Hz/pixel. Multiple MRI runs were averaged in samples with multiple MRI acquisitions. All acquisitions have proton density, T2* and some amount of T1 weighting; thus, the contrast is qualitatively similar.

Table 1 Demographic information for all (n = 21) samples

Sample	Age (years)	Sex	Hemisphere	BB stage	PMI (hours)	Brain weight (grams)	MRI resolution (μm^3)
1	49	M	LH	0	3	1300	–
2	52	F	LH	0	15	1250	120
3	58	M	RH	0	25	1154	150
4	61	M	RH	0	23	1310	120
5	61	M	RH	0	159	1325	120
6	63	M	LH	0	< 12	1359	120
7	64	M	RH	0	15	1230	–
8	65	M	LH	0	25	1309	–
9	68	M	RH	0	17	1320	100
10	59	M	LH	I	20	1319	150
11	68	M	RH	I	< 24	1595	100
12	72	F	RH	I	105	1400	–
13	73	F	RH	I	23	1356	150
14	79	M	LH	I	15	1200	150
15	60	F	LH	II	2	1328	150
16	60	F	LH	II	n/a	> 1380	–
17	62	M	LH	II	16	1370	150
18	75	M	LH	II	24	1187	120
19	78	M	LH	II	24	1320	100
20	70	M	LH	III	24	1250	200
21	77	F	LH	III	34	1300	120

Samples include a subset with both histological validation and ex vivo high-resolution MRI scans (n = 11). Five LC samples had only MRI data (#6, 10, 14, 17, and 19) and five had only histology data (#1, 7, 8, 12, and 16). Samples have been ordered by age and diagnosis. All samples were cognitive controls at the time of death

Abbreviations: F = female, M = male, MRI = ex vivo MRI, RH = right hemisphere, LH = left hemisphere

Histology procedures

Brainstem blocks were cryoprotected in a 20% glycerol, 2% dimethyl sulfoxide solution for at least two weeks. Tissue blocks were sectioned in the horizontal plane at 50 µm on a freezing sliding microtome (Leica Biosystems Richmond Inc, Buffalo Grove, IL), collected serially, and stored at −20 °C in cryoprotectant. Blockface photographs were collected at each serial section using a Canon EOS-1D Mark IV camera (Canon, Tokyo, Japan), which was mounted above the microtome.

Native (unstained) sections

Unstained sections were prepared to evaluate native neuromelanin appearance in each sample (Fig. 1a). Tissue sections were mounted on gelatin-coated slides and air-dried overnight; no staining was performed. Slides were then dehydrated in increasing concentrations of ethanol, cleared in xylene, and coverslipped using Permount (Fisher Scientific, Fair Lawn, NJ).

Histological validation of locus coeruleus labels

LC manual labels from the MRI were validated with histology (native) sections for the location and size of the LC (Fig. 1). Manual labels were drawn (A.H.) with three resources: cross-referencing histology staining, the robust neuromelanin contrast evident in high-resolution MRI, and guidance of expert neuroanatomist (J.C.A.). Our dataset included samples with both histology and MRI (n = 11) for a total of 16 histology and 16 MRI samples (Table 1). MRI voxels in FLASH images appear dark in LC due to the presence of neuromelanin [15, 41]. In the five samples without histology, the LC was labeled based on neuromelanin MRI contrast and measurements (i.e. size and location in the pons) previously determined in histology samples.

Immunohistochemistry

Immunohistochemistry experiments were performed as previously described in [46]. Briefly, free-floating tissue sections in 12-well plates were washed three times in phosphate-buffered saline (PBS) and incubated with 0.5% Triton X-100 in 3% hydrogen peroxide for 20 min to quench endogenous peroxides, then rinsed in PBS three times for 5 min each. Tissue was blocked using 5% nonfat dry milk in PBS for 2 h at room temperature and rinsed in PBS for 1 min. Monoclonal phosphorylated

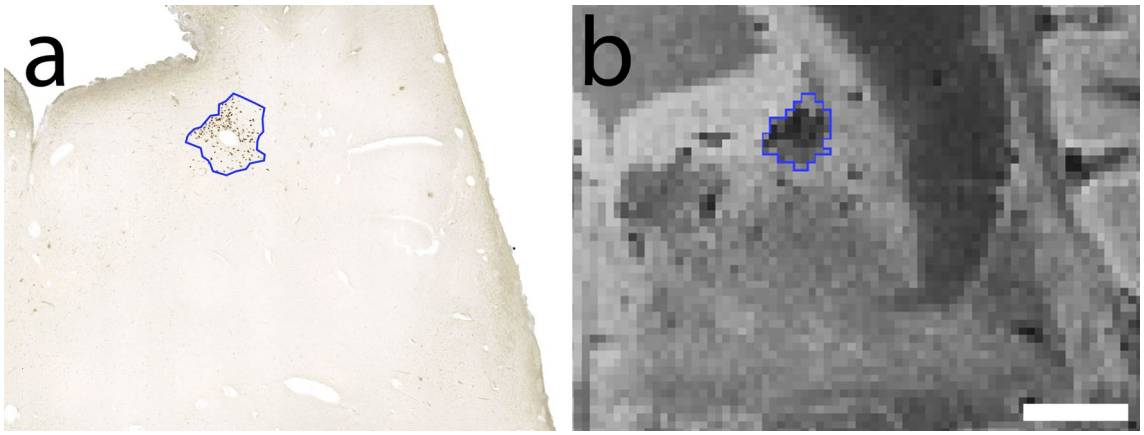

Fig. 1 Histologically-validated locus coeruleus in ex vivo MRI at macroscale. LC (blue outline) in unstained axial histology section (**a**) and corresponding high-resolution ex vivo MRI label (**b**) at midpoint in upper LC. **a** shows the native neuromelanin and **b** shows the dark contrast in FLASH image. Both images represent sample #3. Resolution for ex vivo MRI is 150 mm isotropic. Scale bar = 2 mm

tau antibody CP13 (gift from P. Davies, Albert Einstein College of Medicine; New York; USA Cat# CP13, RRID:AB_2314223) antibody was diluted 1:200 in 1.5% normal goat serum (NGS) (Jackson Immunoresearch, West Grove, PA) in PBS and incubated overnight at 4 °C. Goat anti-mouse secondary antibody was diluted in 1.5% NGS in PBS at 1:200 and incubated for one hour at room temperature (Jackson Immunoresearch, West Grove, PA). Tissue was subsequently washed with PBS. To visualize the staining, tissue was incubated with chromogen 3′3-diaminobenzidine (DAB kit, Vector Laboratories, Burlingame, CA) in a solution of 0.003% 3′3-diaminobenzidine and 0.3% hydrogen peroxide for 7 min. Tissue was rinsed three times in 0.1 M phosphate buffer prior to mounting on slides and air drying overnight. Immunostained sections were dehydrated in increasing concentrations of ethanol solutions, cleared with xylene, and coverslipped with Permount (Fisher Scientific, Fair Lawn, NJ). Negative and positive controls were included in each experiment.

Locus coeruleus anatomical subdivisions in upper pons

We subdivided the LC into three rostrocaudal sublevels based on neighboring anatomical landmarks (Fig. 2). All subdivisions reside within the upper pons. First, rostral LC (Fig. 2b, f and i) extends from approximately the caudal limit of the inferior colliculi to the inferior-most decussation of the superior cerebellar peduncles (SCP). The middle LC segment (Fig. 2c, g and j) extends from the SCP decussation to the beginning of middle cerebellar peduncle, superiorly. Third, caudal LC (Fig. 2d, h and k) extends from the superior limit of the middle cerebellar peduncle landmark to its end, typically where the middle cerebellar peduncle meets the cerebellum in axial view.

Locus coeruleus MRI – manual labels

The LC was manually labeled on axial MRI slices using Freeview, the MRI visualization software included with FreeSurfer v7.4.1 (https://surfer.nmr.mgh.harvard.edu/). LC labels were manually subdivided according to our defined sublevels of the upper pons. All MRI scans were oriented in anatomical position (Fig. 2a and e) to ensure consistency in length measurements. LC lengths were calculated as the distance between the superior-most and inferior-most axial slices in the label. Volume measurements of the LC label were exported from Freeview and recorded (Supplementary Table 1).

Semi-quantitative tau grades—assessing severity in locus coeruleus and cortex

The medial temporal lobe was processed separately to determine the BB staging for all samples. Samples were assigned between BB 0-III based on the tau severity and location [16]. We assessed tau severity within the upper pons at a granular level. This approach was deliberate to enhance specificity and sensitivity, both subregionally and pathologically. Tau severity was assessed semi-quantitatively on three slides per pontine sublevel. The sections were stained with CP13, as described above, and generated a total of nine slides per sample within the upper pons for a fine-grained approach. We built upon Braak's subcortical pretangle stages; LC *Grades 1–2* and *3–4* expand upon stages 'a' and 'b' [18, 36] by accounting for the presence and severity of either dystrophic neurites (Fig. 3g) or somatic tangles (Fig. 3h–j) in the LC, respectively. Five semi-quantitative tau grades (scores

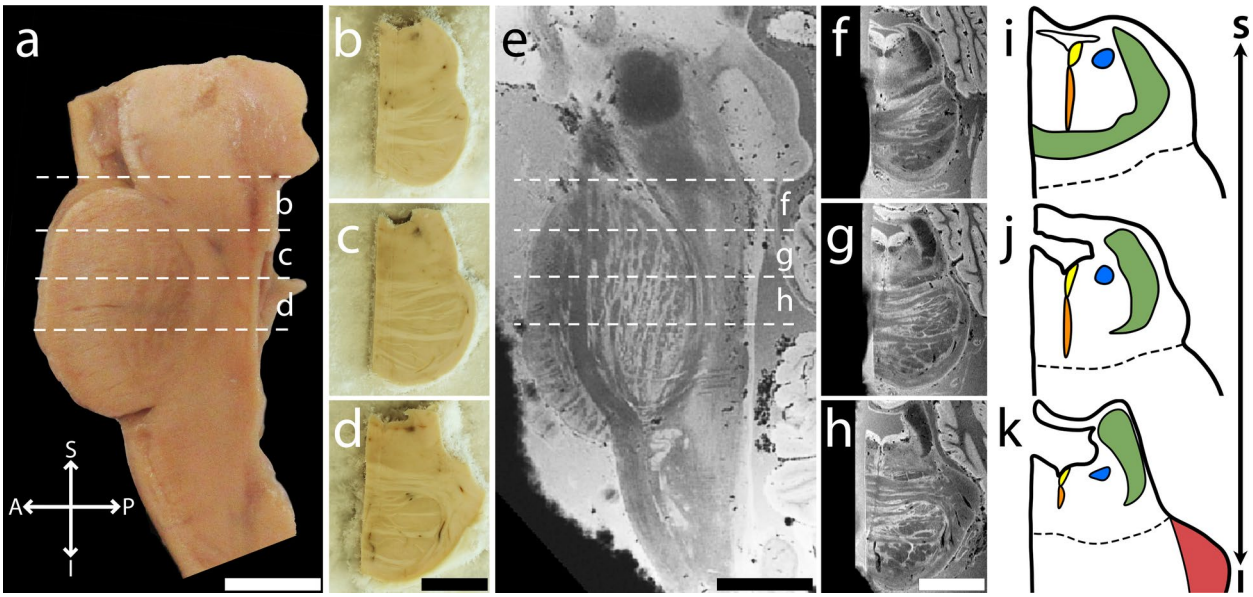

Fig. 2 Anatomically-defined upper pons sublevels. Sagittal view shows specimen (58-year-old male) in gross (**a**) and in high-resolution ex vivo MRI (**e**) with axial blockface images (**b**–**d**), axial MRI images (**f**–**h**), and color-coded upper pons schemata (**i**–**k**). Images **b**–**d** and **f**–**h** were taken from within the subregions indicated in (**a**) and (**e**), respectively. Panels **b**–**d**, **f**–**h**, and **i**–**k** define and depict sublevels containing rostral (**b**, **f**, **i**), middle (**c**, **g**, **j**), and caudal LC (**d**, **h**, **k**). **i**–**k** Color code for pons schemata: locus coeruleus (blue), caudal dorsal raphe (yellow), median raphe (orange), superior cerebellar peduncle (green), and middle cerebellar peduncle (red). Scale bars = 1 cm

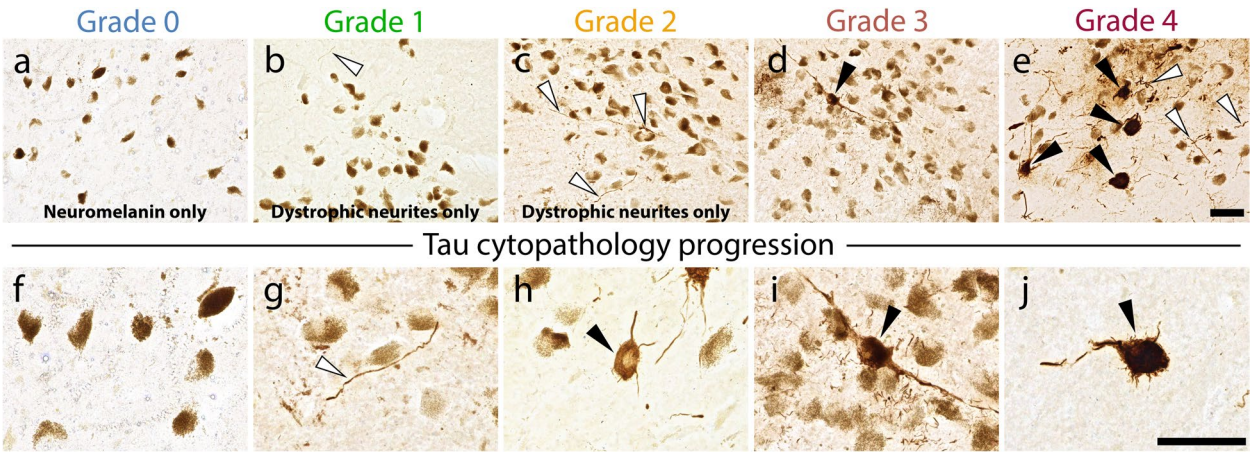

Fig. 3 Semi-quantitative tau severity grades and cytopathology progression in the locus coeruleus. **a**–**e** LC tau severity *Grades 0–4* in rostral (**a**, **b**) and middle LC (**c**–**e**) sections. **f** Unstained, native neuromelanin rich LC neurons. **g**–**j** Progression of LC tau pathology from **g** dystrophic neurites to **h**–**j** somas filled with increasing amounts of tau. Note the spiked somatic protrusions characteristic of severe LC tangles in **j**. Scale bar = 100 µm

0–4) for LC were established here. *Grade 0* refers to tissue with no CP13 reactive material (no tau; dystrophic neurites or tangles) in the LC or its periphery. Given that our samples were postmortem and older, this grade was not observed in our dataset. Figure 3a shows an unstained histology section as a placeholder to demonstrate negative tau material. *Grade 1* indicates no tangles, but a few small, isolated dystrophic neurites (e.g., typically less than three neurites in total) (Fig. 3b). *Grade 2* signifies a greater prevalence of dystrophic neurites but still without tangles (Fig. 3c). *Grade 3* designates a couple of tangles (e.g., typically less than three in the LC), with a mild-to-moderate number of dystrophic neurites (Fig. 3d). *Grade 4* demarcates the most severe LC pathology, with an abundance of tangles and dystrophic neurites in and immediately around the LC (Fig. 3e). Often in *Grade 4*, tangles undertook a darker stain appearance and expressed more somatic protrusions when compared

to *Grade 3*. Supplementary Table 2 shows the tau grades for all samples.

Assessing severity in dorsal raphe

DRc severity was graded on a different five-point (0–4) scale on the same sections used to assess the LC. *Grade 0* signifies tissue devoid of any CP13 immunoreactivity (Supplementary Fig. 1a). *Grade 1* shows only dystrophic neurites in the DRc without tangles (Supplementary Fig. 1b). *Grade 2* includes dystrophic neurites and isolated tangles (e.g., one to two tangles per section) (Supplementary Fig. 1c). *Grade 3* represents moderate tangles (e.g., three to four per section) and mild dystrophic neurite prevalence (Supplementary Fig. 1d). *Grade 4* indicates the most severe with at least five or more tangles in the DRc accompanied by abundant dystrophic neurites (Supplementary Fig. 1e).

Statistical analysis

Ordinal mixed-effects models were constructed in R (v4.4.1) using the "ordinal" R-package to quantify the association between tau severity (*Grade 0–4*) and either BB stage or rostrocaudual sublevel. To account for dependent data (i.e., multiple slices per subject), a random-intercept was included for each subject. For tau severity comparisons between BB stages, sublevel was included as a random effect. Likelihood ratio tests were calculated to determine whether the fixed effect had a significant effect on the response variable. If found to be significant, post hoc testing with Tukey contrasts was used to compare the means of the mixed model. We employed non-parametric tests to assess group differences because the data were not normally distributed. Mann–Whitney U Tests were applied to determine the differences between medians for our quantitative (MRI) data. Kruskal–Wallis tests with Dunn's multiple comparison test were used to determine group differences in our semi-quantitative data. Spearman correlations assessed the association between LC anatomy (volume and length) and tau severity. Significance threshold for statistical tests was set at $p < 0.05$. Data presentation was conducted using GraphPad Prism (GraphPad Software, version 10.3.1, www.graphpad.com).

Results

High-resolution MRI locus coeruleus spatial volumes and dimensions

These experiments represent a sensitive and specific evaluation of LC subdivision sizes based on high-resolution ex vivo MRI. Our manual labels extended slightly beyond the darkest voxels to accurately reflect the average LC width as determined by validated histology (~ 1.5 mm in diameter, Fig. 1). Figure 4a shows the location of the LC in sagittal MRI view relative to other brainstem regions and with a color-coded subdivision schema. Figure 4b provides a closer view of the rostrocaudal LC subdivisions schema (light blue—rostral, blue—middle, dark blue—caudal). Figure 4c–f illustrate 3D reconstruction isoforms of representative samples at each BB stage (BB 0-III). BB III samples were excluded from our quantitative comparisons to focus on the preclinical stage (BB 0-II), as AD symptoms tend to arise at this pathology stage [7, 17, 23]. We detected significant whole volume differences between BB 0 and BB II (Fig. 4g, 30.0% smaller volumes in BB II, $p = 0.0381$, Mann–Whitney U test). At the same level, we observed a trend in whole length differences between the same two groups (Fig. 4k, 14.2% shorter lengths in BB II, $p = 0.0667$, Mann–Whitney U test) but these observations were not significant. Both trends were most pronounced in rostral LC volume (49.2% smaller rostral LC volumes between BB 0 and BB II, $p = 0.0381$, Mann–Whitney U test) and length (25.2% smaller rostral LC lengths between BB 0 and BB II, $p = 0.0667$, Mann–Whitney U test). BB III samples appeared to follow a similar trend (Supplementary Fig. 2). No significant volume and length differences due to hemisphere (volume: $p = 0.2667$; length: $p = 0.2667$, Mann–Whitney U test) were observed in control samples (BB 0).

Tau severity mapping in locus coeruleus

Tau pathology in the LC became more dense and severe during the progression through preclinical AD stages, specifically between BB I and II (Fig. 5b; 37.6% increase, $p < 0.0001$, Dunn's multiple comparison test). Based on abnormally phosphorylated tau (CP13) in three sections per pons sublevel (rostral, middle, and caudal), we created a tau severity heatmap (Fig. 5a). This heatmap represents a highly sensitive spatial matrix with detailed severity for the LC. There were no *Grade 0* LC sections in our dataset. All somatic neurofibrillary tangles in the LC and DRc either partially or fully filled the soma; we did not observe any mature "flame-like" tangles (no ghost tangles). Supplementary Fig. 3 shows the comparisons including BB III cases. Both BB 0 and BB I samples showed significantly different tau severities than BB II (Fig. 5b; $p < 0.0001$, Dunn's multiple comparison test; Supplementary Table 3), reflecting greater tau accumulation occurring at BB II, prior to the symptomatic stage beginning at BB III. LC sublevel did not have a significant effect on tau severity (Fig. 5c, $p = 0.2762$, Kruskal–Wallis test). However, when including BB IIIs in the comparison and accounting for pseudoreplications, we observed a significant difference between rostral and middle LC severity, with greater severity affecting the middle component (Supplementary Table 4; 11.3% greater, $p = 0.0289$, Tukey multiple comparisons test). We observed that significant

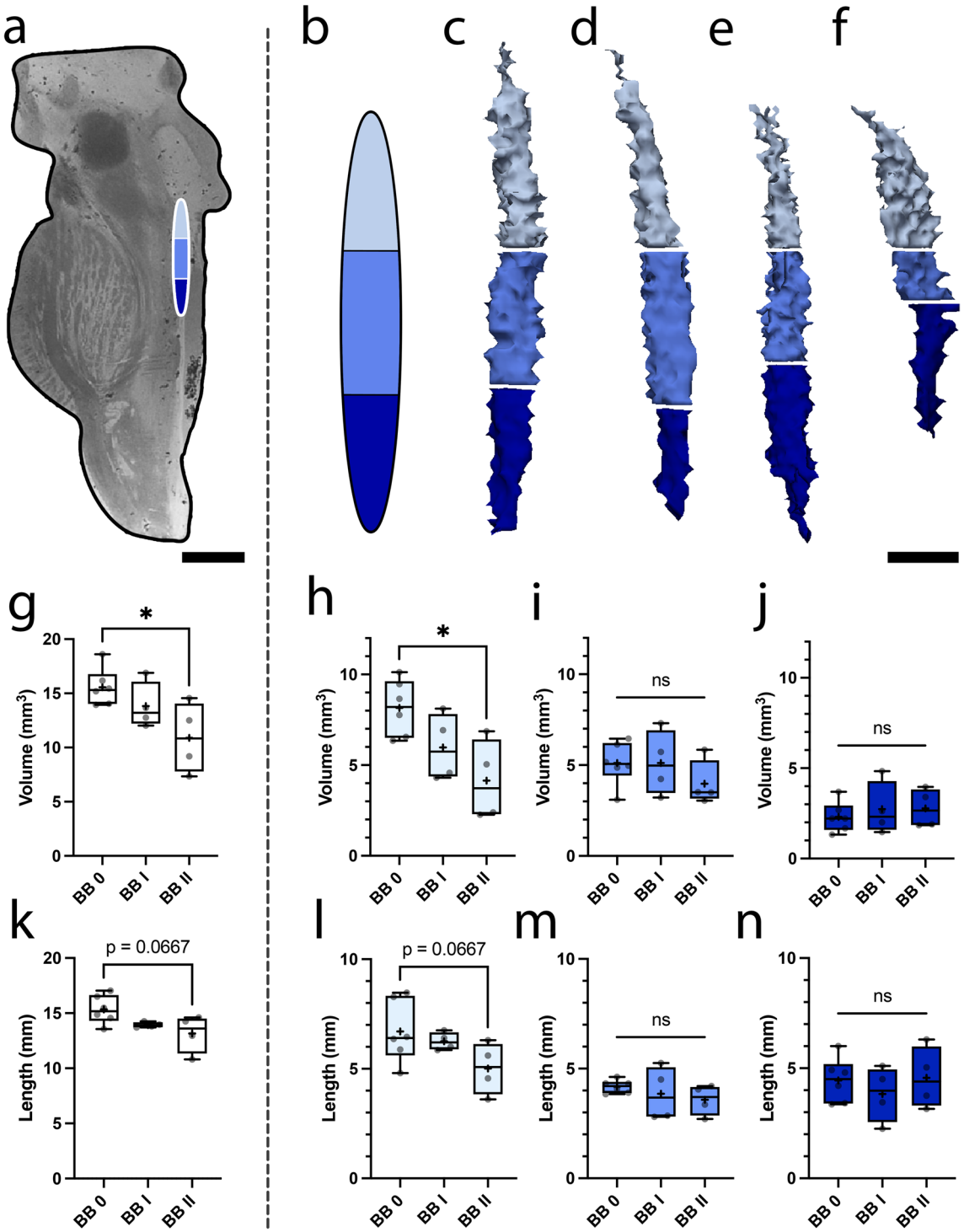

Fig. 4 Locus coeruleus in MRI. **a** Brainstem schema in midsagittal ex vivo MRI, localizing LC. Scale bar = 1 cm. **b** The three LC rostrocaudal sublevels: light blue–rostral, blue–middle, dark blue–caudal. **c**–**f** 3D label reconstructions in aged control (BB 0) and earliest stages of Alzheimer's disease neuropathologic change (BB I-III) in samples #3, 13, 18, and 21. Median volumes (**g**–**j**) and lengths (**k**–**n**) for whole LC and its rostral, middle, and caudal portions, respectively, with interquartile range shown. Significant differences between BB 0 and BB II observed in whole (Panel g, $p = 0.0381$, Mann–Whitney U test) and rostral LC volumes (Panel h, $p = 0.0381$, Mann–Whitney U test). Plus (+) symbols indicate mean. Scale bar = 2 mm

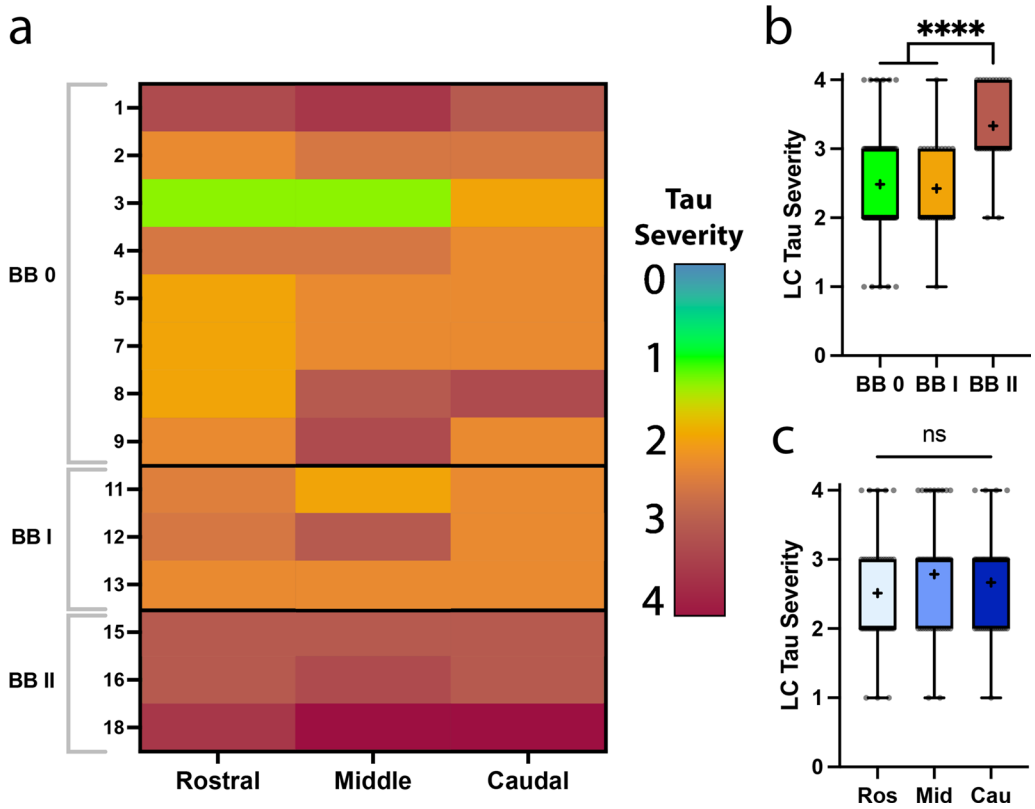

Fig. 5 Tau burden in locus coeruleus at earliest Braak and Braak stages. **a** Heatmap of mean LC tau severity scores at each rostrocaudal sublevel. Panels **b** and **c** show median semi-quantitative tau burden by Braak stage (**b**; significant differences between BB 0 and BB I vs. BB II, $p < 0.0001$, Dunn's multiple comparison test) and sublevel (**c**) for preclinical (BB 0-II) samples. Plus (+) symbols indicate mean

abnormal tau accumulation (Fig. 5b) occurs with significant LC structural atrophy (Fig. 4g) at BB II, in the preclinical phase.

Tau severity in dorsal raphe

Abnormally phosphorylated tau was present in the DRc of all samples, including BB 0 samples, and was most severe at the rostral-most subdivision. We demonstrate a tau severity matrix for DRc samples at the same rostrocaudal upper pons sublevels as the LC (Supplementary Fig. 4). Not surprisingly, tau appeared most severe in the BB II group in DRc, but this was not a significant difference (Supplementary Fig. 4b; $p = 0.7306$, Kruskal–Wallis test; Supplementary Table 5). When comparing tau severities at each upper pons sublevel, the rostral-most DRc segment bore significantly more severe tau burden than both the middle and caudal portions (Supplementary Fig. 4c; 37.3% decrease in rostral vs. middle DRc $p = 0.0267$, 58.2% decrease in rostral vs. caudal DRc $p < 0.0001$, Dunn's multiple comparison test; Supplementary Table 6). The middle DRc trended towards greater severity than the caudal level, but this lacked significance (Supplementary Fig. 4c, $p = 0.1251$, Dunn's multiple comparison test).

Tau severity heatmaps on 3D locus coeruleus reconstructions

Once we semi-quantitatively graded LC tau severity on all histopathology sections, we averaged these data per sample, per sublevel. These average tau grades from validated histopathology sections were manually mapped onto the 3D MRI reconstructions to generate LC pathology heatmaps (n = 11 samples) (Fig. 6a–k) at the preclinical stage. These reconstructions demonstrate LC tau severity in the preclinical window (e.g., non-Alzheimer's diagnosed or Alzheimer's disease Neuropathologic Change, ADNC). Figure 6l shows the averaged data from preclinical samples (BB 0-II) and mapped onto an LC model. The average tau severities at rostral, middle, and caudal LC levels were 2.51, 2.79, and 2.67, respectively (n = 14). Sublevel had no statistical effect on tau severity for this subset ($p = 0.2762$, Kruskal–Wallis test). Representative samples from each observed tau severity grade were included to illustrate the early and specific pathology (Fig. 6m–p).

Correlations between locus coeruleus spatial dimensions and tau severity

LC volume and length measurements at each rostrocaudal sublevel were paired with their corresponding average tau severities for (n = 11) validated samples (i.e., with both histology and MRI data). Spearman correlations between tau severity and MRI volume (Supplementary Fig. 5a, r = −0.1699, $p = 0.344$) and MRI length (Supplementary Fig. 5b, r = −0.1460, $p = 0.4176$) revealed nonsignificant inverse relationships for both correlations.

Discussion

The LC has been a region of interest in understanding Alzheimer's disease development due to its early tau pathology. Our study used a combination of histopathology and ex vivo MRI to investigate the LC and DRc in the early stages of AD. We created manual LC labels to report accurate LC volume and length changes within the preclinical window of Alzheimer's disease. Our data provided precise measures given available histological validation and having complete, high-resolution, 3D MR images of the whole LC without missing slices. Pathologically, we observed phosphorylated tau in the LC for all cases, confirming that the LC is an early site for tau accumulation prior to the cortex. We noted several statistically significant trends reflecting subregional atrophy (Fig. 4) and tau accumulation (Fig. 5) within our cases. This was striking given the narrow window of preclinical (BB I-II) stages evaluated. We also expanded upon the Braak subcortical pretangle stages 'a', 'b' and 'c' [18, 36] to account for the variation in tau severity and applied this grading structure to the three rostrocaudal subregions of the LC and DRc. Our findings culminated in 3D reconstructions of tau severity heatmaps with subregional LC specificity and sensitivity. These data reflect a systematic and rigorous approach to pathology assessment at its earliest stage.

We sought to introduce three anatomically defined rostrocaudal sublevels within the upper pons to assess neuronal vulnerabilities in the LC and DRc during these preclinical stages of AD. LC topography is a relevant feature in AD due to its cortical connections, studied extensively in rats [51, 47, reviewed in 52] that have recently been observed in humans [74]. In both rats and humans, projections from the rostral half of the LC innervate key regions in memory formation and AD vulnerability within the medial temporal lobe (e.g. hippocampus). Therefore, designating a rigorous system for subdividing the LC would allow for more consistent studies into regional differences within the nucleus. Moreover, by establishing and defining anatomical landmarks that can be identified in in vivo MRI scans, we provide additional groundwork for future investigations to assess the LC clinically. Additionally, we implemented a comprehensive system for assessing tau severity in the LC and DRc. Previous studies have used measures such as qualitative scores [33, 62], binary scoring criteria for the presence or absence of either dystrophic neurites or somatic tangles [17, 18], and quantitative means [3, 9, 28] to gauge tau burden. Therefore, we devised a semi-quantitative system for grading tau pathology in both the LC and DRc that includes aspects from many of these past studies.

High-resolution ex vivo MRI scans were utilized to measure the volume and length of the LC. Our measures were likely similar to in vivo sizes due to minimal post-fixation tissue shrinkage, based on previous reports [43, 61, 68]. Brain weight did not have a significant effect on LC volume or length (data not shown). We observed no significant inter-hemispheric differences in either LC volume or length, consistent with previous studies [12, 21, 31, 32]. The LC has sexually dimorphic characteristics [49, 77], but due to low sample size, sex differences could not be accurately assessed. Our manual LC labels were validated with ground truth histological data (Fig. 1) and by comparing our measurements against previous reports (Supplementary Table 7). Our control data align with these reported ranges; however, our volume measures appeared smaller than was expected based on the findings from [44] and [55]. This disagreement is likely due to differences in labeling protocols.

LC volume decreased significantly with BB stages (Fig. 4g) with the effect being most pronounced at rostral LC (Fig. 4h). Our findings indicate that rostral LC is selectively vulnerable to atrophy early in AD progression. This appears to conflict with our histopathology findings, which showed greater tau severity in the middle LC compared to its rostral end. However, it has been shown that tangle burden is not entirely reflective of neuronal loss in AD [2, 35], which may explain the trend we observed.

(See figure on next page.)

Fig. 6 Histopathologically-validated locus coeruleus tau severity maps. **a**–**k** Heatmaps in ex vivo MRI reconstructions based on average tau severity grades in respective samples #2, 11, 15, 20, 3, 13, 18, 21, 4, 5, and 9. Age and sex are shown at bottom for each sample. **l** Average (n = 14) tau severity at each sublevel (rostral LC mean ± s.d. = 2.51 ± 0.81; middle = 2.79 ± 0.84; caudal = 2.67 ± 0.69) from preclinical (BB 0-II) histopathology samples. Note the darker hue in the middle third of LC indicating more severe tau burden. **m**–**p** Tau (CP13 +) histopathology stains demonstrate LC tau severity grades 1–4 at middle LC in samples #3, 11, 4, and 21. **a**–**k** Scale bar = 2 mm. **m**–**p** Scale bars = 100 µm

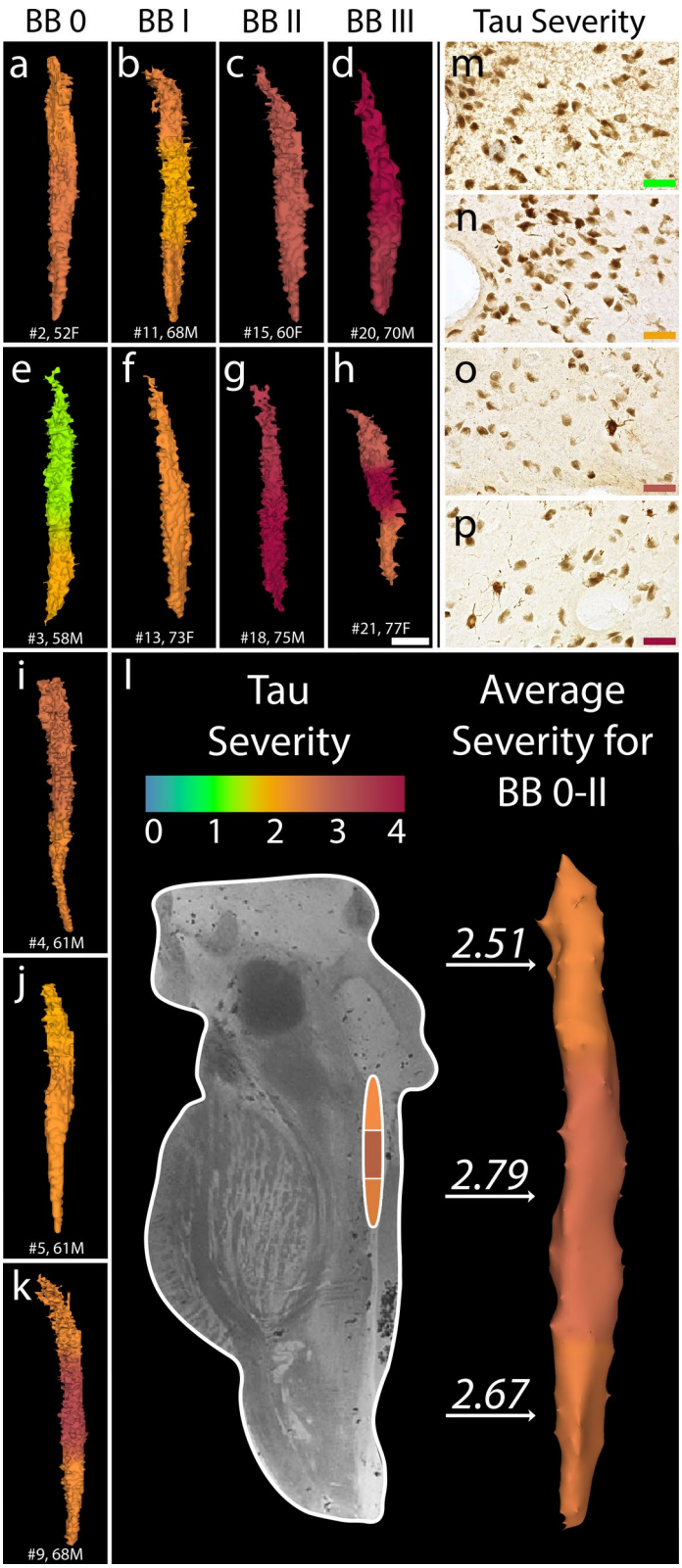

Fig. 6 (See legend on previous page.)

Notable increases in LC tau severity were observed between BB 0, BB I, and BB II (Fig. 5b). Due to the low sample size of BB III cases, statistics were performed with and without these samples. However, no such significant differences were noted between BB II and III (Supplementary Fig. 3d). These data suggest that severe tau accumulation in the LC arises between BB I and BB II. When comparing the three rostrocaudal sublevels in BB 0-III, we observed significantly greater tau severity in the middle LC compared to its rostral portion (Supplementary Table 4); however, this significant difference was not present without BB III samples (Fig. 5c). Taken together, our findings indicate that the regionality of LC tau accumulation becomes relevant between BB II and BB III stages. In the DRc, we observed greater tau severity between BB 0 and BB III samples (Supplementary Fig. 4d). Tau severity differences between BB stages were difficult to assess in the DRc due to the low sample size. More notably, we observed a significant gradient in DRc tau severity across the three rostrocaudal sublevels in BB 0-II samples, where tau burden was more severe rostrally than caudally (Supplementary Fig. 4c). This implies a highly specific regional vulnerability within the DRc and warrants a future stereological study to confirm its validity. It is possible that the DRc intrinsically contains fewer cells at its caudal-most end, which would account for the less severe pathological burden observed caudally in our data.

Previous studies have reported different tau severity trends within the early BB stages of the whole LC. [9] and [3] both report higher overall LC tau severity in stages BB III-IV samples compared to BB I-II, while [5] report an uptick in severity between BB I and II with no significant differences between BB IIs and IIIs, the latter being consistent with our results (Fig. 5b). Our agreement with [5] and disagreement with [9] and [3] may be attributed to the different tau severity scoring systems employed, since [9] and [3] used quantitative systems while [5] used a semi-quantitative grading scale. The similarities in our results confirm the high sensitivity of semi-quantitative tau severity assessments and suggest that severe tau accumulation appears in the LC prior to BB III.

There is a strong need for accurate LC MRI labels in vivo, as the connection between the LC and AD has led to several studies that utilized the LC's natural MR contrast to assess its integrity through signal contrast ratios. Significant contrast ratio differences between AD and controls [38, 45] and specific increases in maximum signal intensity within the rostral LC of older individuals [13, 22] suggest that LC contrast ratios are useful measures for assessing LC pathology in vivo. Studies by [19, 20, 30, 40] reported an association between LC integrity and AD pathology, and demonstrated correlations between lower LC intensity and increased cortical tau prevalence (measured via PET imaging), greater beta-amyloid deposition (via PET), and worsening cognitive/neuropsychiatric symptoms. Other studies investigated the impact of different LC subregions in AD symptom development in vivo. Dahl et al. [24] and [14] demonstrated lower rostral LC integrity to be associated with worse memory performance and AD dementia, respectively, further supporting the pathological relevance of LC subregionality in AD. In all, these studies identified the LC as a specific site affected in early AD progression, highlighting the need for further investigations into LC integrity as a reliable early AD biomarker.

The DR is primarily composed of serotonergic neurons and innervates the hippocampus, entorhinal cortex, and neocortex, among other brain regions [1, 42, 53]. The DR normally functions in mood regulation and sleep, both of which, similar to the LC, become dysregulated early in AD progression and frequently lead to depressive symptoms [60, reviewed in 65 and 26]. Past studies into the DR and AD reported early tau accumulation appearing at BB I and greater severity occurring at later (BB III+) Braak stages [28, 62]. Our data agree with [62], and we expanded on their study; we established a more detailed DR grading scale and included control samples in our dataset. Our results indicate the presence of tau pathology in the DRc in the control samples at approximately the same severity as BB I-II (Supplementary Fig. 4b). A shift in tau severity only occurs at BB III (Supplementary Fig. 4d), suggesting a correlation between AD symptom onset and severe tau accumulation in the DRc. However, these observations lacked statistical significance given the low sample size.

Abnormal tau presence at this earliest stage corroborates the findings of [33] and supports the DR as one of the earliest sites to accumulate tau, but it is still uncertain whether the LC or DR is the first site for tau accumulation [65]. Grinberg and colleagues [33] demonstrated that the DR exhibits pathology during BB 0, with their youngest sample being from a 54-year-old individual. In [18], two samples between the ages of 1 and 10 had phosphorylated tau in the LC but not the DR. Other regions (e.g. substantia nigra, ventral tegmental area, periaqueductal gray, amygdala, thalamus, and hypothalamus) contained tau pathology at BB 0 in samples as young as 21 years old [67]. However, the same study [67] reported that both the LC and DR exhibited greater pathological burden compared to the other regions examined, suggesting early vulnerability of the two nuclei. In the present study, we observed tau outside of the LC and DRc in the pons, consistent with previous findings from [18] who observed AT8-immunoreactive neurites in the central tegmental tract, the superior cerebellar peduncle, and the midbrain

tegmentum, lateral to the medial longitudinal fasciculus. Taken together, this suggests that the earliest AD pathological change does not always start in either the LC or DR, instead, these two nuclei together may represent the most common sites of early AD pathology.

Our study comes with some limitations. First, our low sample size for BB III cases, which often represents the earliest stage when memory impairment manifests clinically [7, 17, 23]. Our low BB III sample size limits the conclusions we can draw concerning brainstem pathology present at AD symptom onset. Second, the DRc was not always included in the sample when the brain hemispheres were bisected. As a result, we had a smaller subset (n = 9) of samples to study. The low availability of DRc tissue, as well as our lack of rostral DR sections, limits our insight into DR tau pathology during preclinical AD.

Our study also has notable strengths. By focusing on cognitively unimpaired BB 0-III samples, we have noted pathological changes within the LC and DR that may be affected by the conversion from preclinical to symptomatic AD. We leveraged high-resolution ex vivo MRI scans to build histologically validated LC labels, which further corroborated previous LC volume and length measurements [10, 21, 31, 32, 69] in rigorous detail. Our findings highlight the potential for in vivo MRI LC measurements to serve as biomarkers for tracking preclinical AD progression, which may soon become a reality through the development of higher-resolution in vivo LC imaging [56, 59, 78]. Our histology data were highly sensitive on account of the multiple sections stained per LC sublevel and the CP13 antibody used to detect early pretangle material [76]. Overall, this study's strength was combining histology and MRI data on the same samples *and* at the same time point (i.e. postmortem). This allowed us the ability to compare tau pathology against structural atrophy with highly specific regionality throughout the entire LC.

Conclusion

We combined histopathology and high-resolution MRI to study the LC and DRc in the preclinical and early symptomatic stages of AD. Our 3D MRI reconstruction results show a significant downward trend in LC volume with higher BB stages, specifically within the rostral LC segments. Our histology results confirm the early presence of abnormally phosphorylated tau in both the LC and DRc in cases without cortical tau (BB 0). Progressive increase in tau severity was visualized throughout the preclinical (BB I-II) and early symptomatic (BB III) stages of AD. Our findings elucidate regional hotspots for tau burden within the middle LC and rostral DRc at these early stages. This investigation also demonstrates the pathological changes occurring within these two brainstem nuclei during the early stages of AD before dementia onset. This stage has the most significant potential for developing effective clinical applications or interventions.

Abbreviations

3D	Three-dimensional
AD	Alzheimer's disease
ADNC	Alzheimer's disease neuropathologic change
BB	Braak and Braak stage
DR	Dorsal raphe nucleus
DRc	Dorsal raphe, caudal subnucleus
FLASH	Fast-low-angle-shot
LC	Locus coeruleus
MRI	Magnetic resonance imaging
NGS	Normal goat serum
PBS	Phosphate-buffered saline
PET	Positron emission tomography
PMI	Postmortem interval
SCP	Superior cerebellar peduncle
TE	Echo time
TR	Repetition time

Supplementary Information

The online version contains supplementary material available at https://doi.org/10.1186/s40478-025-01957-6.

Supplementary material 1.

Supplementary material 2.

Supplementary material 3.

Supplementary material 4.

Acknowledgements

We thank our brain donors, who made this work possible. We appreciate Dr. Peter Davies's generosity to researchers for the CP13 tau antibody.

Author contributions

A.H.: conceptualization, formal analysis, investigation, figure design, writing, reviewing, and editing. S.C.: investigation, reviewing, and editing. N.M.: formal analysis, reviewing, editing. E.C.S.: investigation, reviewing, and editing. A.V.D.K.: investigation, reviewing. B.F. resources, reviewing. C.M.: resources, reviewing. L.K.: resources, reviewing. M.F.: resources, reviewing. J.C.A.: conceptualization, formal analysis, investigation, figure design, supervision, funding acquisition, project administration, writing, reviewing, and editing.

Funding

Funding for this work was supported by National Institute Health grants: for JCA: NIA R01AG057672, R01AG072056, RF1AG082223.

Availability of data and materials

All supporting data are available in the paper and Supplementary Materials.

Declarations

Ethics approval and consent to participate

Autopsy consent was obtained, and tissue was collected with allowance for tissue to be used in research under a protocol approved by the Institutional Review Board of MassGeneralBrigham.

Consent for publication

Not applicable.

Competing interests

The authors declare no competing interests.

Author details
[1]Department of Radiology, Athinoula A. Martinos Center for Biomedical Imaging, Massachusetts General Hospital, 149 Thirteenth St, Suite 2301, Charlestown, MA 02129, USA. [2]Harvard Medical School, Boston, MA 02115, USA. [3]Computer Science and Artificial Intelligence Laboratory (CSAIL), Massachusetts Institute of Technology, Cambridge, MA 02139, USA. [4]C.S. Kubik Laboratory for Neuropathology, Massachusetts General Hospital, Boston, MA 02114, USA.

Received: 17 December 2024 Accepted: 13 February 2025
Published online: 28 February 2025

References

1. Abrams JK, Johnson PL, Hollis JH, Lowry CA (2004) Anatomic and functional topography of the dorsal raphe nucleus. Ann NY Acad Sci 1018(1):46–57. https://doi.org/10.1196/annals.1296.005
2. Andrade-Moraes CH, Oliveira-Pinto AV, Castro-Fonseca E, Da Silva CG, Guimaraes DM, Szczupak D, Parente-Bruno DR, Carvalho LRB, Polichiso L, Gomes BV, Oliveira LM, Rodriguez RD, Leite REP, Ferretti-Rebustini REL, Jacob-Filho W, Pasqualucci CA, Grinberg LT, Lent R (2013) Cell number changes in Alzheimer's disease relate to dementia, not to plaques and tangles. Brain 136(12):3738–3752. https://doi.org/10.1093/brain/awt273
3. Andrés-Benito P, Fernández-Dueñas V, Carmona M, Escobar LA, Torrejón-Escribano B, Aso E, Ciruela F, Ferrer I (2017) Locus coeruleus at asymptomatic early and middle Braak stages of neurofibrillary tangle pathology. Neuropathol Appl Neurobiol 43(5):373–392. https://doi.org/10.1111/nan.12386
4. Aston-Jones G, Waterhouse B (2016) Locus coeruleus: from global projection system to adaptive regulation of behavior. Brain Res 1645:75–78. https://doi.org/10.1016/j.brainres.2016.03.001
5. Attems J, Thomas A, Jellinger K (2012) Correlations between cortical and subcortical tau pathology. Neuropathol Appl Neurobiol 38(6):582–590. https://doi.org/10.1111/j.1365-2990.2011.01244.x
6. Augustinack JC, van der Kouwe AJW, Blackwell ML, Salat DH, Wiggins CJ, Frosch MP, Wiggins GC, Potthast A, Wald LL, Fischl BR (2005) Detection of entorhinal layer II using Tesla magnetic resonance imaging. Ann Neurol 57(4):489–494. https://doi.org/10.1002/ana.20426
7. Bancher C, Jellinger K, Lassmann H, Fischer P, Leblhuber F (1996) Correlations between mental state and quantitative neuropathology in the Vienna Longitudinal Study on Dementia. Eur Arch Psychiatry Clin Neurosci 246(3):137–146. https://doi.org/10.1007/BF02189115
8. Bari A, Xu S, Pignatelli M, Takeuchi D, Feng J, Li Y, Tonegawa S (2020) Differential attentional control mechanisms by two distinct noradrenergic coeruleo-frontal cortical pathways. Proc Natl Acad Sci 117(46):29080–29089. https://doi.org/10.1073/pnas.2015635117
9. Beardmore R, Durkin M, Zayee-Mellick F, Lau LC, Nicoll JAR, Holmes C, Boche D (2024) Changes in the locus coeruleus during the course of Alzheimer's disease and their relationship to cortical pathology. Neuropathol Appl Neurobiol 50(1):e12965. https://doi.org/10.1111/nan.12965
10. Beardmore R, Hou R, Darekar A, Holmes C, Boche D (2021) The Locus coeruleus in aging and alzheimer's disease: a postmortem and brain imaging review. J Alzheimer's Dis 83(1):5–22. https://doi.org/10.3233/JAD-210191
11. Beason-held LL, Horwitz B (2002) Aging Brain. In: Ramachandran VS (ed) Encyclopedia of the human brain. Academic Press, San Diego, pp 43–57. https://doi.org/10.1016/B0-12-227210-2/00009-1
12. Beckers E, Riphagen JM, Van Egroo M, Bennett DA, Jacobs HIL (2024) Sparse asymmetry in locus coeruleus pathology in alzheimer's disease. J Alzheimer's Dis 99(1):105–111. https://doi.org/10.3233/JAD-231328
13. Betts MJ, Cardenas-Blanco A, Kanowski M, Jessen F, Düzel E (2017) In vivo MRI assessment of the human locus coeruleus along its rostrocaudal extent in young and older adults. Neuroimage 163:150–159. https://doi.org/10.1016/j.neuroimage.2017.09.042
14. Betts MJ, Cardenas-Blanco A, Kanowski M, Spottke A, Teipel SJ, Kilimann I, Jessen F, Düzel E (2019) Locus coeruleus MRI contrast is reduced in Alzheimer's disease dementia and correlates with CSF Aβ levels. Alzheimer's Dement: Diagnosis, Assess Dis Monit 11(1):281–285. https://doi.org/10.1016/j.dadm.2019.02.001
15. Betts MJ, Kirilina E, Otaduy MCG, Ivanov D, Acosta-Cabronero J, Callaghan MF, Lambert C, Cardenas-Blanco A, Pine K, Passamonti L, Loane C, Keuken MC, Trujillo P, Lüsebrink F, Mattern H, Liu KY, Priovoulos N, Fliessbach K, Dahl MJ, Hämmerer D (2019) Locus coeruleus imaging as a biomarker for noradrenergic dysfunction in neurodegenerative diseases. Brain: A J Neurol 142(9):2558–2571. https://doi.org/10.1093/brain/awz193
16. Braak H, Braak E (1991) Neuropathological stageing of Alzheimer-related changes. Acta Neuropathol 82(4):239–259. https://doi.org/10.1007/BF00308809
17. Braak H, Del Tredici K (2011) The pathological process underlying Alzheimer's disease in individuals under thirty. Acta Neuropathol 121(2):171–181. https://doi.org/10.1007/s00401-010-0789-4
18. Braak H, Thal DR, Ghebremedhin E, Del Tredici K (2011) Stages of the pathologic process in Alzheimer disease: age categories from 1 to 100 years. J Neuropathol Exp Neurol 70(11):960–969. https://doi.org/10.1097/NEN.0b013e318232a379
19. Bueichekú E, Diez I, Kim C-M, Becker JA, Koops EA, Kwong K, Papp KV, Salat DH, Bennett DA, Rentz DM, Sperling RA, Johnson KA, Sepulcre J, Jacobs HIL (2024) Spatiotemporal patterns of locus coeruleus integrity predict cortical tau and cognition. Nat Aging. https://doi.org/10.1038/s43587-024-00626-y
20. Cassidy CM, Therriault J, Pascoal TA, Cheung V, Savard M, Tuominen L, Chamoun M, McCall A, Celebi S, Lussier F, Massarweh G, Soucy J-P, Weinshenker D, Tardif C, Ismail Z, Gauthier S, Rosa-Neto P (2022) Association of locus coeruleus integrity with Braak stage and neuropsychiatric symptom severity in Alzheimer's disease. Neuropsychopharmacology 47(5):1128–1136. https://doi.org/10.1038/s41386-022-01293-6
21. Chan-Palay V, Asan E (1989) Alterations in catecholamine neurons of the locus coeruleus in senile dementia of the Alzheimer type and in Parkinson's disease with and without dementia and depression. J Comp Neurol 287(3):373–392. https://doi.org/10.1002/cne.902870308
22. Clewett DV, Lee T-H, Greening S, Ponzio A, Margalit E, Mather M (2016) Neuromelanin marks the spot: Identifying a locus coeruleus biomarker of cognitive reserve in healthy aging. Neurobiol Aging 37:117–126. https://doi.org/10.1016/j.neurobiolaging.2015.09.019
23. Consensus recommendations for the postmortem diagnosis of Alzheimer's disease (1997). The National Institute on Aging, and Reagan Institute Working Group on Diagnostic Criteria for the Neuropathological Assessment of Alzheimer's Disease. Neurobiol Aging, 18(4), S1–S2. https://doi.org/10.1016/S0197-4580(97)00057-2
24. Dahl MJ, Mather M, Düzel S, Bodammer NC, Lindenberger U, Kühn S, Werkle-Bergner M (2019) Rostral locus coeruleus integrity is associated with better memory performance in older adults. Nat Hum Behav 3(11):1203–1214. https://doi.org/10.1038/s41562-019-0715-2
25. Dahl MJ, Mather M, Werkle-Bergner M, Kennedy BL, Guzman S, Hurth K, Miller CA, Qiao Y, Shi Y, Chui HC, Ringman JM (2022) Locus coeruleus integrity is related to tau burden and memory loss in autosomal-dominant Alzheimer's disease. Neurobiol Aging 112:39–54. https://doi.org/10.1016/j.neurobiolaging.2021.11.006
26. Demir EA, Tutuk O, Dogan H, Tumer C (2019) Depression in Alzheimer's disease: the roles of cholinergic and serotonergic systems. In: Wisniewski T (ed) Alzheimer's Disease. Codon Publications, Brisbane (AU)
27. Edlow BL, Mareyam A, Horn A, Polimeni JR, Witzel T, Tisdall MD, Augustinack JC, Stockmann JP, Diamond BR, Stevens A, Tirrell LS, Folkerth RD, Wald LL, Fischl B, van der Kouwe A (2019) 7 Tesla MRI of the ex vivo human brain at 100 micron resolution. Sci Data 6(1):244. https://doi.org/10.1038/s41597-019-0254-8
28. Ehrenberg AJ, Nguy AK, Theofilas P, Dunlop S, Suemoto CK, Di Lorenzo Alho AT, Leite RP, Rodriguez RD, Mejia MB, Rüb U, Farfel JM, de Lucena Ferretti-Rebustini RE, Nascimento CF, Nitrini R, Pasqualucci CA, Jacob-Filho W, Miller B, Seeley WW, Heinsen H, Grinberg LT (2017) Quantifying the accretion of hyperphosphorylated tau in the locus coeruleus and dorsal raphe nucleus: The pathological building blocks of early Alzheimer's disease. Neuropathol Appl Neurobiol 43(5):393–408. https://doi.org/10.1111/nan.12387
29. Elobeid A, Soininen H, Alafuzoff I (2012) Hyperphosphorylated tau in young and middle-aged subjects. Acta Neuropathol 123(1):97–104. https://doi.org/10.1007/s00401-011-0906-z
30. Engels-Domínguez N, Riphagen JM, Van Egroo M, Koops EA, Smegal LF, Becker JA, Prokopiou PC, Bueichekú E, Kwong KK, Rentz DM, Salat DH, Sperling RA, Johnson KA, Jacobs HIL (2024) Lower locus coeruleus

integrity signals elevated entorhinal tau and clinical progression in asymptomatic older individuals. Ann Neurol 96(4):650–661. https://doi.org/10.1002/ana.27022
31. Fernandes P, Regala J, Correia F, Gonçalves-Ferreira AJ (2012) The human locus coeruleus 3-D stereotactic anatomy. Surg Radiol Anat 34(10):879–885. https://doi.org/10.1007/s00276-012-0979-y
32. German D, Walker B, Manaye K, Smith W, Woodward D, North A (1988) The human locus coeruleus: Computer reconstruction of cellular distribution. J Neurosci 8(5):1776–1788. https://doi.org/10.1523/JNEUROSCI.08-05-01776.1988
33. Grinberg LT, Rüb U, Ferretti REL, Nitrini R, Farfel JM, Polichiso L, Gierga K, Jacob-Filho W, Heinsen H, Group, B. B. B. S. (2009) The dorsal raphe nucleus shows phospho-tau neurofibrillary changes before the transentorhinal region in Alzheimer's disease. A precocious onset? Neuropathol Appl Neurobiol 35(4):406–416. https://doi.org/10.1111/j.1365-2990.2008.00997.x
34. Grudzien A, Shaw P, Weintraub S, Bigio E, Mash DC, Mesulam MM (2007) Locus coeruleus neurofibrillary degeneration in aging, mild cognitive impairment and early Alzheimer's disease. Neurobiol Aging 28(3):327–335. https://doi.org/10.1016/j.neurobiolaging.2006.02.007
35. Gómez-Isla T, Hollister R, West H, Mui S, Growdon JH, Petersen RC, Parisi JE, Hyman BT (1997) Neuronal loss correlates with but exceeds neurofibrillary tangles in Alzheimer's disease. Ann Neurol 41(1):17–24. https://doi.org/10.1002/ana.410410106
36. Harley CW, Walling SG, Yuan Q, Martin GM (2021) The 'a, b, c's of pretangle tau and their relation to aging and the risk of Alzheimer's Disease. Semin Cell Dev Biol 116:125–134. https://doi.org/10.1016/j.semcdb.2020.12.010
37. Heneka MT, Nadrigny F, Regen T, Martinez-Hernandez A, Dumitrescu-Ozimek L, Terwel D, Jardanhazi-Kurutz D, Walter J, Kirchhoff F, Hanisch U-K, Kummer MP (2010) Locus ceruleus controls Alzheimer's disease pathology by modulating microglial functions through norepinephrine. Proc Natl Acad Sci 107(13):6058–6063. https://doi.org/10.1073/pnas.0909586107
38. Hou R, Beardmore R, Holmes C, Osmond C, Darekar A (2021) A case-control study of the locus coeruleus degeneration in Alzheimer's disease. Eur Neuropsychopharmacol 43:153–159. https://doi.org/10.1016/j.euroneuro.2020.12.013
39. Iannitelli AF, Weinshenker D (2023) Riddles in the dark: Decoding the relationship between neuromelanin and neurodegeneration in locus coeruleus neurons. Neurosci Biobehav Rev 152:105287. https://doi.org/10.1016/j.neubiorev.2023.105287
40. Jacobs HIL, Becker JA, Kwong K, Engels-Domínguez N, Prokopiou PC, Papp KV, Properzi M, Hampton OL, Uquillas F, Sanchez JS, Rentz DM, Fakhri GE, Normandin MD, Price JC, Bennett DA, Sperling RA, Johnson KA (2021) In vivo and neuropathology data support locus coeruleus integrity as indicator of Alzheimer's disease pathology and cognitive decline. Sci Transl Med 13(612):eabj2511. https://doi.org/10.1126/scitranslmed.abj2511
41. Keren NI, Taheri S, Vazey EM, Morgan PS, Granholm A-CE, Aston-Jones GS, Eckert MA (2015) Histologic validation of locus coeruleus MRI contrast in post-mortem tissue. Neuroimage 113:235–245. https://doi.org/10.1016/j.neuroimage.2015.03.020
42. Köhler C, Steinbusch H (1982) Identification of serotonin and non-serotonin-containing neurons of the mid-brain raphe projecting to the entorhinal area and the hippocampal formation. A combined immunohistochemical and fluorescent retrograde tracing study in the rat brain. Neuroscience 7(4):951–975. https://doi.org/10.1016/0306-4522(82)90054-9
43. Kotrotsou A, Bennett DA, Schneider JA, Dawe RJ, Golak T, Leurgans SE, Yu L, Arfanakis K (2014) Ex vivo MR volumetry of human brain hemispheres. Magn Reson Med 71(1):364–374. https://doi.org/10.1002/mrm.24661
44. Lechanoine F, Jacquesson T, Beaujoin J, Serres B, Mohammadi M, Planty-Bonjour A, Andersson F, Poupon F, Poupon C, Destrieux C (2021) WIKI-BrainStem: an online atlas to manually segment the human brainstem at the mesoscopic scale from ultrahigh field MRI. Neuroimage 236:118080. https://doi.org/10.1016/j.neuroimage.2021.118080
45. Li M, Liu S, Zhu H, Guo Z, Zhi Y, Liu R, Jiang Z, Liang X, Hu H, Zhu J (2022) Decreased locus coeruleus signal associated with Alzheimer's disease based on neuromelanin-sensitive magnetic resonance imaging technique. Front Neurosci. https://doi.org/10.3389/fnins.2022.1014485
46. Llamas-Rodríguez J, Oltmer J, Greve DN, Williams E, Slepneva N, Wang R, Champion S, Lang-Orsini M, Fischl B, Frosch MP, van der Kouwe AJW, Augustinack JC (2022) Entorhinal subfield vulnerability to neurofibrillary tangles in aging and the preclinical stage of Alzheimer's disease. J Alzheimer's Dis 87(3):1379. https://doi.org/10.3233/JAD-215567
47. Loughlin SE, Foote SL, Bloom FE (1986) Efferent projections of nucleus locus coeruleus: topographic organization of cells of origin demonstrated by three-dimensional reconstruction. Neuroscience 18(2):291–306. https://doi.org/10.1016/0306-4522(86)90155-7
48. Lucey BP, McCullough A, Landsness EC, Toedebusch CD, McLeland JS, Zaza AM, Fagan AM, McCue L, Xiong C, Morris JC, Benzinger TLS, Holtzman DM (2019) Reduced non–rapid eye movement sleep is associated with tau pathology in early Alzheimer's disease. Sci Transl Med 11(474):eaau6550. https://doi.org/10.1126/scitranslmed.aau6550
49. Luckey AM, Robertson IH, Lawlor B, Mohan A, Vanneste S (2021) Sex differences in locus coeruleus: a heuristic approach that may explain the increased risk of Alzheimer's disease in females. J Alzheimer's Dis 83(2):505–522. https://doi.org/10.3233/JAD-210404
50. Malhotra PA (2019) Impairments of attention in Alzheimer's disease. Curr Opin Psychol 29:41–48. https://doi.org/10.1016/j.copsyc.2018.11.002
51. Mason ST, Fibiger HC (1979) Regional topography within noradrenergic locus coeruleus as revealed by retrograde transport of horseradish peroxidase. J Comp Neurol 187(4):703–724. https://doi.org/10.1002/cne.901870405
52. Matchett BJ, Grinberg LT, Theofilas P, Murray ME (2021) The mechanistic link between selective vulnerability of the locus coeruleus and neurodegeneration in Alzheimer's disease. Acta Neuropathol 141(5):631–650. https://doi.org/10.1007/s00401-020-02248-1
53. Michelsen KA, Prickaerts J, Steinbusch HWM (2008) The dorsal raphe nucleus and serotonin Implications for neuroplasticity linked to major depression and Alzheimer's disease. In: G. do Giovann, V. do Matteo, & E. Esposito (Eds.), *Progress in Brain Research*, vol 172, Elsevier, pp 233–264
54. Michelsen KA, Schmitz C, Steinbusch HWM (2007) The dorsal raphe nucleus—from silver stainings to a role in depression. Brain Res Rev 55(2):329–342. https://doi.org/10.1016/j.brainresrev.2007.01.002
55. Mohammadi MS, Planty-Bonjour A, Poupon F, Uszynski I, Poupon C, Destrieux C, Andersson F (2024) ProbaStem, a pipeline towards the first high-resolution probabilistic atlas of the whole human brainstem. Brain Struct Funct 229(1):115–132. https://doi.org/10.1007/s00429-023-02726-8
56. Morris LS, Tan A, Smith DA, Grehl M, Han-Huang K, Naidich TP, Charney DS, Balchandani P, Kundu P, Murrough JW (2020) Sub-millimeter variation in human locus coeruleus is associated with dimensional measures of psychopathology: an in vivo ultra-high field 7-Tesla MRI study. NeuroImage Clinical 25:102148–102148. https://doi.org/10.1016/j.nicl.2019.102148
57. O'Neill E, Harkin A (2018) Targeting the noradrenergic system for anti-inflammatory and neuroprotective effects: implications for Parkinson's disease. Neural Regen Res 13(8):1332. https://doi.org/10.4103/1673-5374.235219
58. Pamphlett R, Kum Jew S (2015) Different populations of human locus ceruleus neurons contain heavy metals or hyperphosphorylated tau: implications for amyloid-β and tau pathology in Alzheimer's disease. J Alzheimer's Dis 45(2):437–447. https://doi.org/10.3233/JAD-142445
59. Priovoulos N, Jacobs HIL, Ivanov D, Uludağ K, Verhey FRJ, Poser BA (2018) High-resolution in vivo imaging of human locus coeruleus by magnetization transfer MRI at 3T and 7T. Neuroimage 168:427–436. https://doi.org/10.1016/j.neuroimage.2017.07.045
60. Pierson SR, Fiock KL, Wang R, Balasubramanian N, Reinhardt J, Khan KM, James TD, Hunter ML, Cooper BJ, Williamsen HR, Betters R, Deniz K, Lee G, Aldridge G, Hefti MM, Marcinkiewcz CA (2024) Tau pathology in the dorsal raphe may be a prodromal indicator of Alzheimer's disease. Mol Psychiatry. https://doi.org/10.1038/s41380-024-02664-9
61. Quester R, Schröder R (1997) The shrinkage of the human brain stem during formalin fixation and embedding in paraffin. J Neurosci Methods 75(1):81–89. https://doi.org/10.1016/S0165-0270(97)00050-2
62. Rüb U, Del Tredici K, Schultz C, Thal DR, Braak E, Braak H (2000) The evolution of Alzheimer's disease-related cytoskeletal pathology in the human raphe nuclei. Neuropathol Appl Neurobiol 26(6):553–567. https://doi.org/10.1046/j.0305-1846.2000.00291.x
63. Salib E, Tadros G (2000) Brain weight in suicide: an exploratory study. Br J Psychiatry 177(3):257–261. https://doi.org/10.1192/bjp.177.3.257

64. Samuels E, Szabadi E (2008) Functional neuroanatomy of the noradrenergic locus coeruleus: its roles in the regulation of arousal and autonomic function part i: principles of functional organisation. Curr Neuropharmacol 6(3):235–253. https://doi.org/10.2174/157015908785777229
65. Simic G, Stanic G, Mladinov M, Jovanov-Milosevic N, Kostovic I, Hof PR (2009) Does Alzheimer's disease begin in the brainstem? Neuropathol Appl Neurobiol 35(6):532–554. https://doi.org/10.1111/j.1365-2990.2009.01038.x
66. Šimić G, Babić Leko M, Wray S, Harrington CR, Delalle I, Jovanov-Milošević N, Bažadona D, Buée L, De Silva R, Di Giovanni G, Wischik CM, Hof PR (2017) Monoaminergic neuropathology in Alzheimer's disease. Prog Neurobiol 151:101–138. https://doi.org/10.1016/j.pneurobio.2016.04.001
67. Stratmann K, Heinsen H, Korf H-W, Del Turco D, Ghebremedhin E, Seidel K, Bouzrou M, Grinberg LT, Bohl J, Wharton SB, den Dunnen W, Rüb U (2016) Precortical phase of Alzheimer's disease (AD)-related tau cytoskeletal pathology. Brain Pathol 26(3):371–386. https://doi.org/10.1111/bpa.12289
68. Teipel SJ, Flatz WH, Heinsen H, Bokde ALW, Schoenberg SO, Stöckel S, Dietrich O, Reiser MF, Möller H-J, Hampel H (2005) Measurement of basal forebrain atrophy in Alzheimer's disease using MRI. Brain 128(11):2626–2644. https://doi.org/10.1093/brain/awh589
69. Theofilas P, Ehrenberg AJ, Dunlop S, Alho AT, Nguy A, Leite REP, Rodriguez RD, Mejia MB, Suemoto CK, de Lucena Ferretti-Rebustini RE, Polichiso L, Nascimento CF, Seeley WW, Nitrini R, Pasqualucci CA, Filho WJ, Rueb U, Neuhaus J, Heinsen H, Grinberg LT (2017) Locus coeruleus volume and cell population changes during Alzheimer's disease progression: a stereological study in human postmortem brains with potential implication for early-stage biomarker discovery. Alzheimer's Dement: J Alzheimer's Assoc 13(3):236–246. https://doi.org/10.1016/j.jalz.2016.06.2362
70. Torso M, Ridgway GR, Valotti M, Hardingham I, Chance SA (2023) In vivo cortical diffusion imaging relates to Alzheimer's disease neuropathology. Alzheimer's Res Ther 15:1–15. https://doi.org/10.1186/s13195-023-01309-3
71. Van Egroo M, Narbutas J, Chylinski D, Villar González P, Maquet P, Salmon E, Bastin C, Collette F, Vandewalle G (2019) Sleep–wake regulation and the hallmarks of the pathogenesis of Alzheimer's disease. Sleep. https://doi.org/10.1093/sleep/zsz017
72. Van Egroo M, van Someren EJW, Grinberg LT, Bennett DA, Jacobs HIL (2024) Associations of 24-hour rest-activity rhythm fragmentation, cognitive decline, and postmortem locus coeruleus hypopigmentation in Alzheimer's disease. Ann Neurol 95(4):653–664. https://doi.org/10.1002/ana.26880
73. Van Egroo M, Riphagen JM, Ashton NJ, Janelidze S, Sperling RA, Johnson KA, Yang H-S, Bennett DA, Blennow K, Hansson O, Zetterberg H, Jacobs HIL (2023) Ultra-high field imaging, plasma markers and autopsy data uncover a specific rostral locus coeruleus vulnerability to hyperphosphorylated tau. Mol Psychiatry 28(6):2412–2422. https://doi.org/10.1038/s41380-023-02041-y
74. Veréb D, Mijalkov M, Canal-Garcia A, Chang Y-W, Gomez-Ruiz E, Gerboles BZ, Kivipelto M, Svenningsson P, Zetterberg H, Volpe G, Betts M, Jacobs HI, Pereira JB (2023) Age-related differences in the functional topography of the locus coeruleus and their implications for cognitive and affective functions. Elife 12:RP87188. https://doi.org/10.7554/eLife.87188
75. Wagatsuma A, Okuyama T, Sun C, Smith LM, Abe K, Tonegawa S (2018) Locus coeruleus input to hippocampal CA3 drives single-trial learning of a novel context. Proc NatL Acad Sci. https://doi.org/10.1073/pnas.1714082115
76. Xia Y, Prokop S, Gorion K-MM, Kim JD, Sorrentino ZA, Bell BM, Manaois AN, Chakrabarty P, Davies P, Giasson BI (2020) Tau Ser208 phosphorylation promotes aggregation and reveals neuropathologic diversity in Alzheimer's disease and other tauopathies. Acta Neuropathol Commun 8:1–17. https://doi.org/10.1186/s40478-020-00967-w
77. Ycaza Herrera A, Wang J, Mather M (2019) The gist and details of sex differences in cognition and the brain: How parallels in sex differences across domains are shaped by the locus coeruleus and catecholamine systems. Prog Neurobiol 176:120–133. https://doi.org/10.1016/j.pneurobio.2018.05.005
78. Ye R, Rua C, O'Callaghan C, Jones PS, Hezemans FH, Kaalund SS, Tsvetanov KA, Rodgers CT, Williams G, Passamonti L, Rowe JB (2021) An in vivo probabilistic atlas of the human locus coeruleus at ultra-high field. Neuroimage 225:117487. https://doi.org/10.1016/j.neuroimage.2020.117487
79. Zucca FA, Segura-Aguilar J, Ferrari E, Muñoz P, Paris I, Sulzer D, Sarna T, Casella L, Zecca L (2017) Interactions of iron, dopamine and neuromelanin pathways in brain aging and Parkinson's disease. Prog Neurobiol 155:96–119. https://doi.org/10.1016/j.pneurobio.2015.09.012

Publisher's Note